Received: 8 April 2025 | Accepted: 21 July 2025

DOI: 10.1111/opo.13564

OPO THE COLLEGE OF OPTOMETRISTS

ORIGINAL ARTICLE

Optimising reaction-time analysis in eye movement perimetry using pooled promptness distributions

Ashwini Venkat Reddy Chanakya[1,2] | **Peter Bremen**[1]

[1]Department of Neuroscience, Erasmus MC, Rotterdam, The Netherlands

[2]Medical Research Foundation, Sankara Nethralaya, Chennai, Tamil Nadu, India

Correspondence
Peter Bremen, Department of Neuroscience, Erasmus MC, Rotterdam, The Netherlands.
Email: p.bremen@erasmusmc.nl

Funding information
Stichting Lijf en Leven, Grant/Award Number: 74_P.Bremen; Oogfonds, Grant/Award Number: 2022-12

Abstract

Reaction-time measurements play a crucial role in assessing cognitive and sensory processing, with applications in functional clinical diagnostics such as eye-movement perimetry (EMP) for the detection of glaucoma. However, reaction-time distributions are typically right-skewed, complicating statistical analysis and requiring large numbers of repetitions for reliable parameter estimation. One well-known transformation to normalise reaction-time distributions is taking their reciprocal, called 'speed' or 'promptness' (unit 1/s). Using the promptness transformation for individual visual-field locations typically normalises the corresponding reaction-time distributions and enables more efficient statistical analysis. This study investigated whether pooling promptness across visual-field locations maintains sufficient normality for robust parameter estimation, even with sparse data typical of clinical applications, such as EMP. The results demonstrate that pooled promptness distributions generally retain normal-like properties in normal vision and glaucoma, allowing for efficient estimation of key distribution parameters (mean and standard deviation) with a minimal number of repetitions. These findings suggest that promptness-based metrics could serve as clinically relevant summary indices for visual-function assessment, similar to mean deviation (MD) in standard perimetry. While the reciprocal transformation of reaction time is well established, its targeted application in visual-field analysis via EMP and the robustness to pooling across stimulus conditions, that is, visual-field locations, has not been explored systematically. This study shows that promptness enables compact, interpretable metrics for EMP, even with sparse data. By reducing data collection demands while preserving statistical rigour, this approach offers a promising framework for enhancing the efficiency and applicability of EMP in clinical and research settings.

KEYWORDS
glaucoma, retina, saccades, visual field, visual-field deficit

INTRODUCTION

Reaction times (RTs) provide a valuable window into cognitive and sensory processes, informing studies on attention,[1–3] decision-making[4,5] and visual processing.[6–8] In clinical and applied settings, reaction-time measurements have been incorporated into diagnostic tools, such as eye-movement perimetry (EMP), which assesses visual-field function based on saccadic reaction times to peripheral stimuli, and which can be used for detecting glaucoma.[9–14]

Typically, reaction-time distributions are right-skewed, making parameter estimation challenging. Standard descriptive statistics such as the mean and standard deviation

are often biased by the long tail of slow responses.[15–17] To account for skewness and the long tail, as well as to understand better the underlying cognitive processes, more complex models have been proposed for the description of reaction-time distributions.[18–21] Alternative models, including ex-Gaussian and drift-diffusion models, offer a more nuanced characterisation of reaction times,[18,20,22,23] but require large numbers of repetitions per condition, which can be impractical in clinical or time-sensitive applications. Consequently, methods that extract key parameters efficiently from limited reaction time data are needed, particularly in clinical applications like EMP.

A potential solution is to analyse the reciprocal of reaction times (1/RT), termed 'speed' or 'promptness',[5,24,25] which often approximates a normal distribution. This transformation facilitates the use of robust statistical techniques. However, when pooling across visual-field locations—where reaction times naturally vary due to eccentricity[26–31] and pathology[10]—promptness values may form mixture distributions rather than a single normal distribution. This investigation addresses the key question of whether these pooled distributions are still 'normal enough' for practical estimation.

We hypothesised that when reaction times are transformed into promptness prior to pooling across visual-field locations, the resulting pooled promptness distribution will approximate a normal distribution, enabling efficient estimation of distribution parameters, even with sparse data typical of clinical application, for example, one measurement per location. These findings will inform future efforts to develop EMP-based summary metrics analogous to mean deviation (MD) in standard perimetry, potentially aiding clinical assessment of visual function.

Key points

- The well-known reciprocal transformation of reaction times (promptness) normalises distributions, facilitating more robust statistical analysis in visual-field assessments.
- Pooled promptness distributions maintain sufficient normality for parameter estimation, enabling efficient analysis with minimal data collection.
- Promptness-based metrics offer a compact and interpretable framework for assessing visual function, potentially enhancing diagnostic efficiency in glaucoma and other visual-field deficits.

METHODS

Ethics approval

All procedures performed in the study involving human participants were in accordance with the ethical standards of the Institutional Research Committee and with the 1964 Helsinki Declaration and its later amendments or comparable ethical standards. The study was approved by the local Medical Ethical Committee of the Erasmus University Medical Centre, Rotterdam, the Netherlands (MEC-2022-0543). Informed consent to participate and for publication was obtained from all participants included in the study.

Participants

A total of 14 participants (8 females, 1 Asian, 13 Caucasian), ranging in age from 24 to 67 years, took part in the experiments (Table 1). Six of the participants were clinically diagnosed with glaucoma (mean age ± SD: 58 ± 16 years; other participants: 45 ± 15 years). Participant 11, brother to participant 10, was not clinically diagnosed with glaucoma but had a genetic predisposition for the disease and presented with enlarged blind spots in both eyes. None of the participants were known to have ophthalmic conditions such as oculomotor nerve palsy, corneal opacities or ptosis, which could potentially interfere with eye tracking. Participants had spherical ametropia <±5.00 D, cylindrical ametropia <−2.00 D and best-corrected visual acuity better than 0.30 logMAR (6/12) for distance and better than 0.50 logMAR (N8) for near. Four of the participants with glaucoma (P10, P12, P13 and P14) had intraocular lenses in one or both eyes. A subset of the participants were familial relatives, and participants 2 and 3 are authors of the study.

Setup

A haploscopic system was used to present visual stimuli independently to the two eyes.[32–34] The system consisted of a PC (Intel i5-6600, 3.30 GHz, 8 GB RAM, Windows 10, dell.com; NVIDIA GeForce GTX 980 Ti, nvidia.com), one Thin-Film Transistor (TFT) monitor (ASUS VG278HE, 27″, 1920 × 1080, 60 Hz, asus.com) for the experimenter, two stimulus TFT monitors (DELL P2419H, 23.8″, 1920 × 1080, 60 Hz, dell.com), two reflective mirrors (height × width: 25 cm × 37 cm), two dichroic mirrors (height × width: 9 cm × 12.5 cm) and an infrared eye tracker (Tobii Pro X3-120, 120 Hz; Tobii AB, tobii.com). All components were mounted in a wooden frame (inside coated black). The monitors were positioned facing downwards and their image was projected on the reflective mirrors, which were inclined at an angle of 45° relative to the monitors. The image from the reflective mirrors was projected onto two participant-facing dichroic mirrors, which were positioned at a 135° angle relative to the participant's viewing direction. The dichroic mirrors reflected visible light from the stimulus monitors and transmitted near-infrared light from the eye tracker mounted behind

TABLE 1 Demographic and clinical characteristics of participants.

Participant ID	Age (years)	Gender	Aetiology	Comments
1	24	F	Normal vision	
2	31	F	Normal vision	Asian; Author
3	43	M	Normal vision	Author
4	45	F	Normal vision	Genetic predisposition
5	50	M	Normal vision	
6	61	M	Normal vision	
7	64	F	Normal vision	Sister of P14 and P13
8	26	M	Glaucoma	Genetic predisposition; Enlarged blind spot in right eye
9	61	F	Glaucoma	
10	63	M	Glaucoma	Brother of P11
11	65	M	Glaucoma?	Brother of P10; Genetic predisposition; Enlarged blind spots in both eyes
12	65	F	Glaucoma	
13	66	F	Glaucoma	Sister of P7 and P14
14	67	F	Glaucoma	Sister of P7 and P13

Abbreviations: F, female; M, male.

the dichroic mirrors at a distance of 65 cm from the participant's eye. The schematic of the experimental setup is illustrated in Figure 1a (also see Meethal et al.[34]). The synchronisation between the screens, that is, target presentation and eye tracker of the haploscopic system was enabled using a high-speed camera (see Appendix A).

During the experiments, participants rested their chin on a soft cushion and their forehead on a cushioned headrest to stabilise their position. They also wore large-diameter spectacle frames without lenses, which were equipped with black blinders to prevent light from the monitors and reflective mirrors from reaching their eyes without obstructing the frontal view.

Visual stimuli

For the experiment, two types of visual stimuli were used, a green fixation circle (radius = 0.88°) and an achromatic target circle (radius = 0.44°). Luminance values of the target, measured at eye level using a 93,560 Luxmeter, BEHA-Amprobe GmbH, beha-amprobe.com, were 10.8 cd/m^2 and 15.8 cd/m^2 (derived from 'cd mode' at 66 cm) against a grey background of 6.2 cd/m^2, resulting in Weber's contrasts (WC) of 74% and 155%. Measurements were taken at eye level due to experimental constraints that prevented direct screen measurements. This approach, while not ideal for self-luminous displays, allowed the capture of light reaching the observer's eye.

A total of 56 target locations across the visual field in oculo-centric coordinates were tested (Figure 2f). Target locations were based on locations used for glaucoma screening.[10,35] Temporal target locations −27°/±3° horizontal/vertical were not tested for the left eye, and locations +27°/±3° horizontal/vertical were not tested for the right eye. While previous work used Cartesian coordinates to define target locations, polar coordinates based on the organisation of the oculomotor system were preferred.[36,37] Saccades are inherently angular movements where the oculomotor system directs the eye to specific points in a circular field of view. Polar coordinates (angle, Φ and eccentricity, R, from a central point) naturally describe these movements, aligning with the eye's rotational motion around the centre of the visual field. Pooling data across different eccentricities (radial distances) and directions becomes straightforward because polar coordinates already separate these dimensions. First, the target locations used for glaucoma detection were transformed to polar coordinates. Next, the Euclidean distances in polar coordinates were calculated between the target locations and reference locations ($\Phi = \{n \mid n \in \mathbb{Z},\ 0 \le n \le 359\}$; $R = \{2.5,5,7.5,10,12.5,15\} \cup \{22.5,25,27.5,30\}$). The new target locations were obtained by minimising the Euclidean distances for each target location (Figure 2f; note that targets fall on the circular lines indicating constant R).

The initial fixation circle was either located straight ahead (horizontal/vertical: 0°/0°) or in one of the four corners of the monitor screen at an eccentricity of 9° from the centre, both horizontally and vertically (Figure 2a–e). Due to the limited size of the stimulus monitors (grey square in Figure 2a–e), eccentric fixation was necessary. Eccentric fixation can impact saccade parameters such as velocity, choice probability and reaction time.[38] In pilot experiments, it was noted that with eccentric fixation, centrally directed saccades were indeed faster than temporally directed saccades by some 10–20 ms (data not shown). While

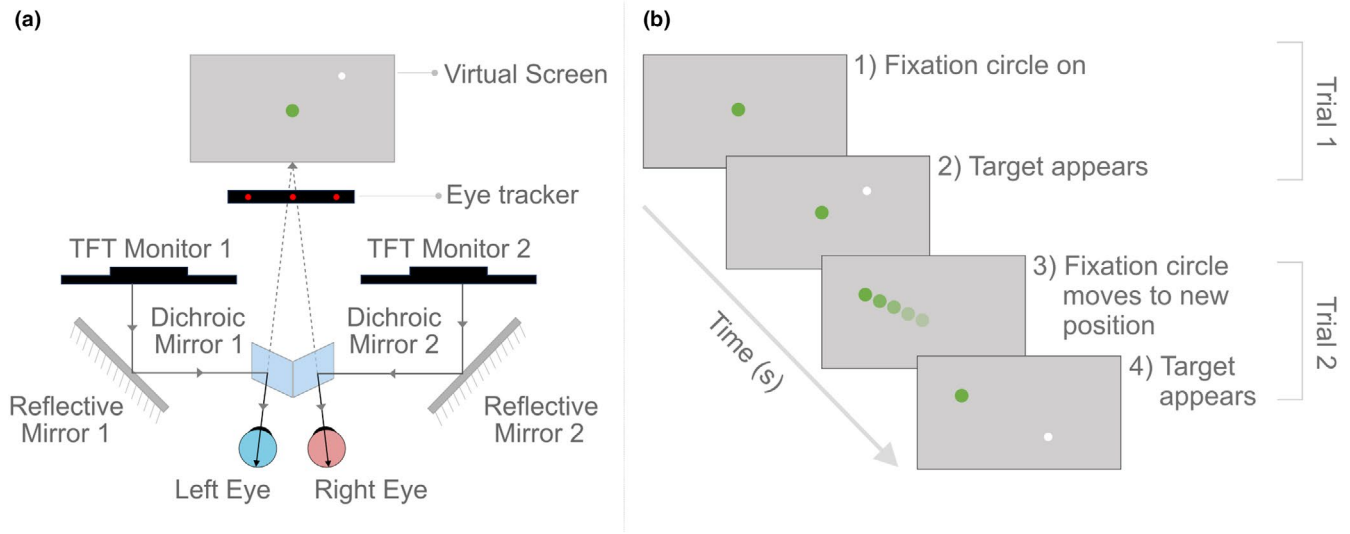

FIGURE 1 Schematic diagram of the haploscope-based eye-tracking setup used for monocular and binocular stimulus presentation (a). The system consists of two Thin-film transistor (TFT) monitors positioned above the participant's line of sight, angled downwards. These project images onto two reflective mirrors placed at 45°, which redirect the visual stimuli horizontally onto dichroic (hot) mirrors facing the participant. The dichroic mirrors selectively reflect visible light while allowing infrared light from the eye tracker to pass through, enabling unobstructed recording of eye movements. The eye tracker is positioned behind the dichroic mirrors, aligned with the eyes. This setup allows for independent monocular or binocular presentation by controlling the stimulus delivered to each monitor. The participant views a virtual screen composed of both monitors' images. Note that the schematic is not to scale and is not drawn in perspective; it is intended to convey optical layout rather than physical geometry (also see Meethal et al.[34]). (b) Schematic overview of the visual-field test paradigm. Step 1: A central fixation stimulus is shown at the start of each trial. Step 2: After a random delay, one target appears at a pseudorandom location, prompting a saccadic eye movement. Peripheral saccadic targets are randomly presented at 54 predefined locations spanning the central and peripheral visual field. Step 3: To expedite data collection, a closed-loop detection system was used. Trials automatically ended when a goal-directed saccade was detected, defined as five consecutive eye-tracker samples within a 5° radius centred on the target. If no saccade was detected or if detection failed, the target remained visible for 1.2 s before the trial ended. For each new trial, the fixation stimulus moved (green circles of varying brightness) to 1–5 randomly chosen fixation locations and the sequence was repeated (step 4).

this difference may impact detailed physiological and behavioural studies of the visuomotor system, it is negligible in clinical diagnostics of the visual system, which compares patient performance to normative data.

With central fixation, one of 24 possible target locations could be presented (Figure 2a), while with the four eccentric fixation conditions, a total of eight target locations were available (Figure 2b–e). That is, the target probability distributions for central (1/24) and eccentric (1/8) fixations were not the same and could have affected reaction times, that is, faster reaction times for eccentric fixations.[25] Due to the size limitations of the available monitors, it was not possible to examine this directly. However, it should be noted that, as expected,[26,28–31] reaction times for peripheral locations in both participants without and with glaucoma were slower than more central ones (e.g., Figures 3 and 4). As discussed above, for detailed oculomotor studies it would be preferable to avoid these differences in stimulus presentation. Since clinical studies rely on comparative analysis, these differences are unlikely to skew diagnostic outcomes.

Behavioural paradigm

All measurements were conducted in a dimly lit and quiet room. A block-randomised experiment was conducted during a session for six viewing conditions, that is, monocular left, monocular right and binocular (not reported here) viewing at two WCs (low = 74%; high = 155%). Each experimental block included 54 target locations, presented randomly and repeated between two and four times. Between 6 and 14 repetitions per location were collected for each participant, except for participant 13, for whom we obtained a minimum of three (right and left eye, WC 155%) and a maximum of six repetitions (right, left and binocular, WC 74%). Here, 'repetition' refers to the number of valid trials recorded per target location, per viewing condition. Each block took 4–10 min to complete, and the entire set of repetitions required around 4 h spread over several days within 3 months. Experimental sessions lasted 1–3 h and were divided into blocks with 5-min breaks, during which the room lights were turned on. For the longer sessions, the breaks were extended to around 1 h.

To calibrate the eye tracker before each block, participants fixated on a red circular target that moved slowly and predictably between nine predefined locations covering the four edges and five central locations on the virtual screen. The eye-tracker system accounted for viewing distance and screen size and converted eye position in normalised screen coordinates into degrees using the Pythagorean theorem.

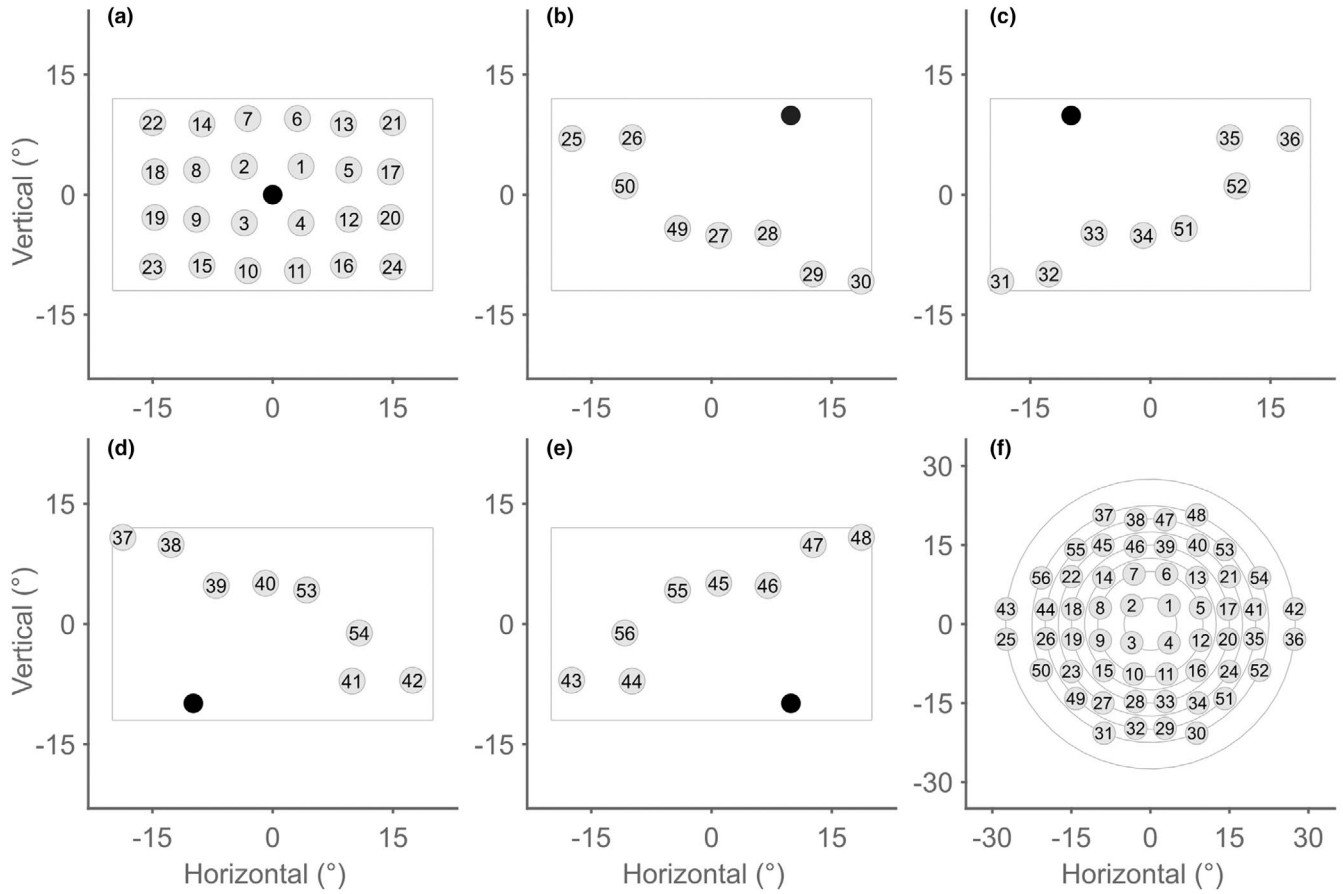

FIGURE 2 Overview of stimulus locations in polar coordinates. (a–e) Locations of the fixation circles (black) and corresponding possible target locations (grey circles with identification number) in monitor-centred coordinates. The monitor dimensions are indicated as a rectangle. Targets are not drawn to scale for legibility. With central fixation (a), one of 24 possible target locations could be presented, while with the four eccentric fixation conditions (b–e), eight target locations were available. This results in a total of 56 target locations across the visual field in oculo-centric coordinates (f). Temporal target locations –27°/±3° horizontal/vertical were not tested for the left eye and locations +27°/±3° horizontal/vertical were not tested for the right eye. Target locations were based on locations used for glaucoma screening but transposed to polar coordinates (iso-eccentricity lines in F; see text for details).

Each block of the visual-field test started with the green fixation circle in the centre of the virtual screen (Figure 1b step 1). The participant had to align their eyes with the fixation circle. After a random delay (10th/50th/90th percentile: 1404/1422/1460 ms), one target would appear at a randomly selected location (Figure 1b step 2). Participants were instructed to move their eyes as quickly and as accurately as possible towards the target. The fixation circle was not removed after the target presentation, matching the paradigm used in eye-movement perimetry.[9] To speed up data collection, a closed-loop system was used to end a trial after the detection of a goal-directed saccade. If five consecutive eye-tracker samples fell within a radius of 5° centred at the target location, the target presentation and the trial ended with an average delay of 60 ms (10th/90th percentile: 31/196 ms). If the participant did not make a saccade or the programme failed to detect the saccades accurately (5% of the trials across all participants and blocks) target presentation and the trial ended 1.2 s after target onset. For subsequent trials, the fixation circle moved to one of the five randomly chosen fixation locations (Figure 2a–e) and the trial sequence was repeated (Figure 1b steps 3 and 4).

Prior to data collection, participants completed a training block (56 target locations, one repetition, WC 155%, binocular viewing). After the training block, an offline analysis was performed to confirm steady fixation before target presentation and accurate saccades within a 10° radius of the target before progressing with data collection. Based on each participant's feedback after the training block, the speed at which the fixation circle moved between trials was adjusted to a comfortable level (18°/s: two participants; 30°/s: 10 participants; 90°/s: two participants).

Data analysis

Extraction of saccadic parameters

Calibrated eye-tracking data were post-processed using a custom-written MATLAB program (version R2024a; MathWorks Inc., mathworks.com). First, right-eye and

left-eye traces were combined by averaging. Next, the data were up sampled to 1 kHz by interpolating the averaged trace using modified Akima cubic Hermite interpolation ('makima' method for MATLAB's 'interp1' function). This algorithm provides smoother, more stable results than nearest-neighbour or linear methods and avoids the oscillations that can occur with spline interpolation. It maintains the continuity of both the signal and its first derivative, which is advantageous for the calculation of saccade velocity. To identify blinks, that is, signal loss, first, the 2D velocity trace of the saccadic eye movement was calculated as the Euclidean norm of the horizontal and vertical eye position derivatives, divided by the time interval between consecutive samples. Candidate blink events were identified using a velocity criterion of 600°/s. A 3-sample running average was applied to smooth out the transitions around the blink event, before interpolating ('*makima*' method) between the onset and offset of the event.

Saccades were detected using peak detection (using the *findpeaks* function in MATLAB with a minimum peak distance of 200 ms) on the velocity trace with a two-step velocity criterion to, first, identify a candidate event (100°/s) and then to localise the onset and offset of the saccade (50°/s). All trials were visually inspected and corrected if necessary (healthy: ~1%; glaucoma: ~28%). For all detected saccades, onset time, offset time, starting horizontal and vertical locations and endpoint horizontal and vertical locations were identified. Reaction time was determined by calculating the difference between the target onset time and the saccade onset time. For analysis, saccades were considered that met the following requirements: (1) first saccade after stimulus onset in a trial, (2) reaction time longer than 100 ms to exclude anticipatory responses and (3) saccadic amplitude within a radius of 5° centred at the fixation circle location and the target location, respectively, in a window of ±10 ms around target onset time and at saccade offset time.

Reciprobit plots for parameter estimation

To normalise reaction time distributions, reaction times (RT) were transformed to their reciprocal (1/reaction time), called 'promptness', *P*, with unit 1/s.[5,25] Mean and standard deviation are suitable descriptors for the resulting promptness distribution. Previous studies have demonstrated the effectiveness of this normalisation for individual conditions across a wide range of reaction-time tasks.[5,25,39,40] Here, it is shown that the promptness distribution pooled across different stimulus conditions, that is, locations in the visual-field task, follows normality. This approach simplifies the statistical summary of reaction-time data across a wide range of experiments since the mean (μ) and standard deviation (σ) become appropriate descriptors and can be used to create global indices of visual-field function, analogous to mean deviation (MD) in standard automated perimetry. To obtain the mean and standard deviation, a reciprobit plot was first constructed.[5] For this plot, promptness is plotted as a function of cumulative probability in probit units, that is, inverse error function (Figure 3k,l). Note that in reciprobit plots—probit plots with promptness on the abscissa—the reciprocal nature of the abscissa justifies this naming convention.[25] In these plots, although promptness is plotted, the axis label is expressed in reaction time units for interpretability. Then, a line was fitted to the reciprobit-transformed data within the 25th and 75th percentiles of the distribution ('*regress*' function in MATLAB). Using the 25th and 75th percentiles of the data offer several advantages, particularly in terms of robustness and accuracy. This approach captures the main trend in the data, focusing on where the majority of the data points lie, rather than the extremes. Using the 25th and 75th percentiles, rather than the entire data range, reduces the influence of extreme values or outliers that can skew results. By focusing on the central portion of the data, the fit remains more robust.

Mean promptness, μ_P is derived from the intercept of the fitted line at 50% of the reciprobit plot. It represents the average speed of visuo-motor processing. While the reciprocal of promptness corresponds to reaction time (RT = 1/*P*), the relationship between mean promptness and mean reaction time is not exact due to Jensen's inequality.[41] Specifically, the mean reaction time, μ_{RT} is generally greater than the reciprocal of the mean promptness:

$$\mu_{RT} \geq \frac{1}{\mu_P}. \quad (1)$$

However, if the promptness distribution is approximately normal with low variance, the error introduced by this approximation may be negligible. For interpretability, $1/\mu_P$ is reported as an approximation of mean reaction time, while noting that it may slightly underestimate the true mean reaction time.

The standard deviation, that is, response variability, is determined from the slope of the fitted line. The promptness standard deviation (σ_P) is transformed back to reaction-time standard deviation (σ_{RT}) as follows:

$$\sigma_{RT} \approx \frac{\sigma_P}{\mu_P^2}. \quad (2)$$

This formula provides an approximation under the assumption that the distribution of promptness values is relatively normal and that the standard deviation is small compared to the mean, which is the case for these data.

Parameter-estimation error

The parameter-estimation error was determined when only a few repetitions per condition were available. First, μ_P and σ_P of the promptness distribution were determined across all 54 target locations for each participant and viewing condition, using all available repetitions per location

(Figure 4). These values served as the reference parameters. Next, distributions were simulated with a varying number of repetitions per target location by randomly selecting measured reaction times for each viewing condition and participant (Figure 5). For instance, when using one repetition per location, a total of 54 promptness values were selected—one from each target location—within a given condition for a participant. This scheme preserved the general visual-field structure. Next, the μ_P and σ_P were determined for this simulated distribution and transformed back to reaction time mean (μ_{RT}) and standard deviation (σ_{RT}). Then, the difference between the reference and simulated parameters was calculated, which was termed the error of the mean, $\boldsymbol{E}_{\mu}$ and the error of the standard deviation, $\boldsymbol{E}_{\sigma}$. To obtain error distributions for both parameters, the error calculation was repeated 1000 times. From these error distributions, the mean, the 95% confidence interval of the mean and the 80%, 95% and 99% confidence intervals of the distribution were calculated (coloured lines and markers in Figure 5b,d,f,h).

Locations with fewer than four repetitions were excluded to prevent biased error estimates in bootstrapping. With low repetition counts, the bootstrapping process repeatedly samples the same values, preventing the algorithm from capturing the natural variability of reaction times across trials. As a result, confidence intervals may become artificially narrow, leading to an overly optimistic view of estimation accuracy, especially at high-confidence thresholds like 95% or 99%. This yields artificially low estimates of the mean and standard deviation errors ($\boldsymbol{E}_{\mu}$ and $\boldsymbol{E}_{\sigma}$), as the bootstrapping procedure cannot account for the potential range of outcomes that additional repetitions would reveal. In contrast, multiple repetitions allow each bootstrap sample to reflect different values from the original distribution, providing a more realistic spread in error estimates.

Since promptness distributions, especially for participants with glaucoma, could deviate from normality, it was of interest to assess how their error distributions deviated from error distributions based on normally distributed data. To that end, normal distributions were simulated based on the reference mean and standard deviation using the same number of maximum repetitions per location measured per participant and viewing condition. The same error analysis was performed for these simulated datasets that were used for the empirical data (grey patches in Figure 5).

Bayesian linear regression fitting

A Bayesian linear regression model was employed to fit a straight line through the origin to the relation mean estimation error, $\boldsymbol{E}_{\mu}$, versus reaction-time standard deviation of the reference set, σ_{RT}, as well as to the relation standard-deviation error, $\boldsymbol{E}_{\sigma}$, versus σ_{RT} using Markov Chain Monte Carlo (MCMC) sampling to estimate the posterior distribution of the slope (Figure 6). All computations and visualisations were conducted in MATLAB, using custom code to implement the Bayesian regression and MCMC sampling. The data consisted of independent variable values σ_{RT} (standard deviation of the reaction-time distribution) and corresponding dependent variable values $\boldsymbol{E}_{\mu}$ (error of the mean reaction time estimate) or $\boldsymbol{E}_{\sigma}$ (error of the reaction time standard-deviation estimate). The likelihood function assumed a Gaussian distribution for the residuals between the observed and predicted values, with the model defined as

$$\boldsymbol{E}_X = m\sigma_{RT} \tag{3}$$

with $\boldsymbol{E}_X$ either $\boldsymbol{E}_{\mu}$ or $\boldsymbol{E}_{\sigma}$ and m indicating the slope of the line. A normal prior distribution $\mathcal{N}(0, 10^2)$ was placed on the slope parameter, reflecting weak prior knowledge. The posterior distribution was proportional to the product of the likelihood and prior. MCMC sampling was performed using the Metropolis–Hastings algorithm with a Gaussian random walk proposal distribution. A total of 10,000 samples were drawn from the posterior. The mean of the posterior samples was used as the maximum a posteriori (MAP) estimate of the slope. The 95% credible interval for the slope was calculated as the 2.5 and 97.5 percentiles of the posterior samples. To visualise the fit, the posterior mean of the slope was used to plot the best-fit line and the credible intervals were represented as a shaded region around the line.

The same Bayesian linear regression approach was used to fit a line to the relation error obtained with a limited target range ($R > 15°$) and error obtained with the full target range for both the mean and standard deviation estimates (Figure 8). The model was defined as:

$$\boldsymbol{E}_l = m\boldsymbol{E}_f + b \tag{4}$$

with m and b, respectively, indicating the slope and intercept of the line and $\boldsymbol{E}_l$ and $\boldsymbol{E}_f$ the error of the mean reaction time estimate, $\boldsymbol{E}_{\mu}$, or of the reaction time standard deviation estimate, $\boldsymbol{E}_{\sigma}$, of the limited target range and full target ranges, respectively.

All statistical analyses were conducted using a significance level (alpha) of 0.01. Consequently, results were considered statistically significant if the corresponding p-value was <0.01. This more stringent alpha criterion was chosen to reduce the likelihood of Type I errors.

RESULTS

Proposed reciprobit analysis for reaction times pooled across conditions

Figure 3 illustrates four steps for analysing reaction time data, each focusing on transforming and interpreting reaction times for healthy participant 3 (left column; left eye; 74% contrast) and participant 10 with glaucoma (right column; left eye; 74% contrast).

In the first row, reaction times to visual stimuli measured across 54 locations were mapped to the visual field using

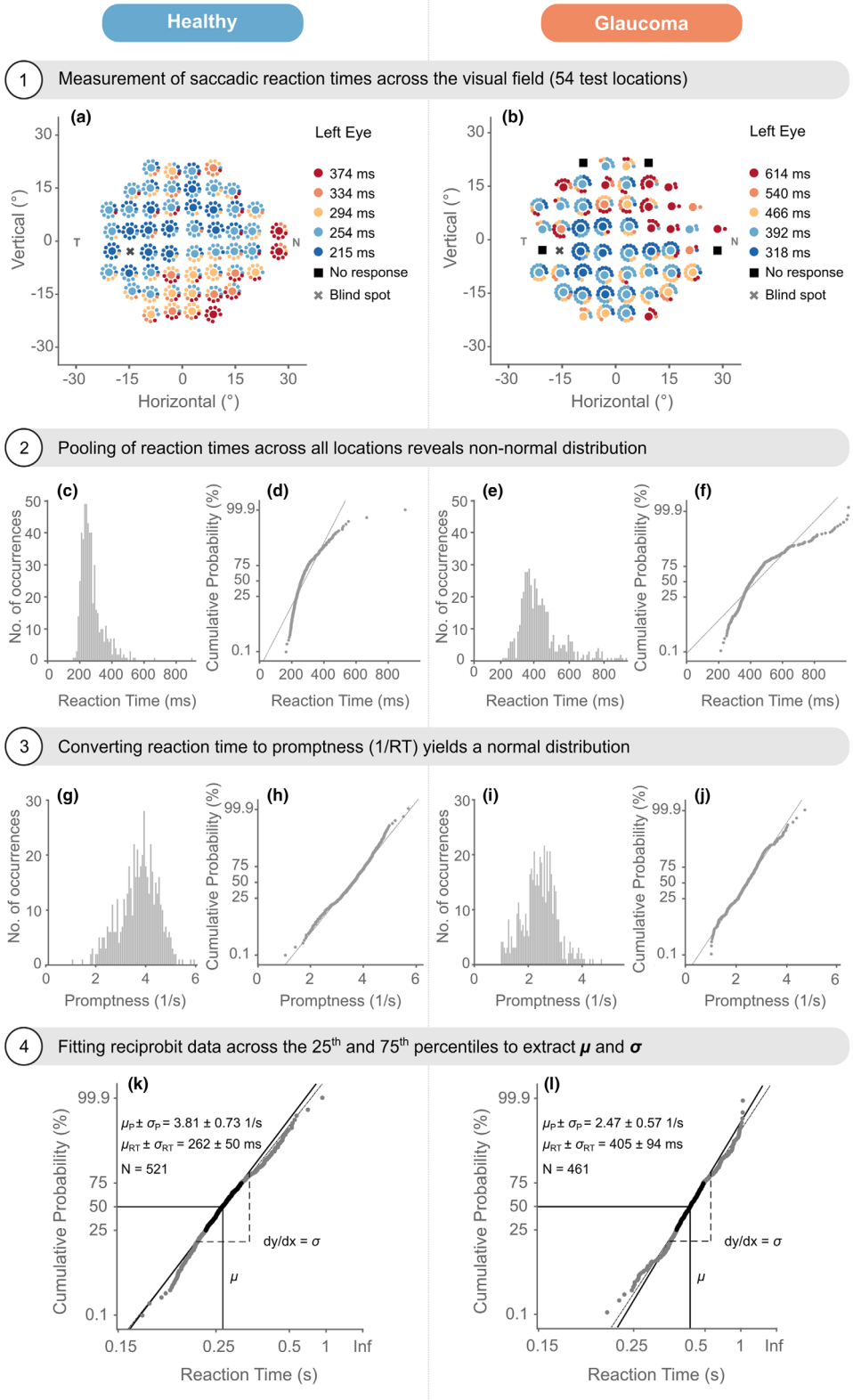

FIGURE 3 Four steps for the analysis of reaction time (RT) data based on promptness and reciprobit analysis. Each step focuses on transforming and interpreting reaction times for two example participants both tested under monocular left and 74% contrast conditions. Left column: Healthy participant 3 (a, c, d, g, h, k). Right column: Participant 10 with glaucoma (b, e, f, i, j, l). For a detailed explanation, see the main text. N, nasal; T, temporal.

colour-coded circles. The hues of the circles ranged from blue (cooler) to red (warmer) indicating fast and slow reaction times, respectively (Figure 3a,b). Large circles represent the median reaction times across all repetitions and small circles represent reaction times for individual repetitions. The median or the mode are more appropriate statistical

descriptors of skewed distributions, like reaction-time distributions.[42] Additionally, the small circles provide information on: (1) the reaction time of individual repetitions and (2) the number of valid saccades across all repetitions. All repetitions are considered valid when the small circles fully surround the large circle. Half-circle coverage indicates 50% valid responses and so on. The blind spot is indicated with a grey 'X' at −15° horizontal and −3° vertical depending on the eye. A filled black square indicates the absence of valid saccades for that location. To facilitate glaucoma detection, two additional nasal (N) locations were measured that were not included on the temporal (T) side.[10,35]

For the healthy participant 3 (Figure 3a), reaction times to low contrast stimuli with the left eye were fast centrally (215–254 ms) and increased towards the periphery, especially in the inferior field (294–374 ms). For most locations, almost 100% of the saccades were valid, indicating an overall intact visual field. In contrast, participant 10 with glaucoma (Figure 3b), assessed in the same manner, exhibited a clear deficit in the superior visual field, a common pattern observed in glaucoma.[43] In that area, reaction times were severely delayed by some 200–300 ms relative to the central and inferior visual field. Moreover, the percentage of valid saccades was reduced to below 50% for some locations and no valid responses were recorded in four locations. As a visualisation tool, the reaction-time map provides an easy-to-parse spatial representation of reaction times, highlighting areas with faster or slower responses, as well as visual-field deficits. For the healthy participant, the map can highlight the well-known difference between central and para-central/peripheral reaction times.[29] For the glaucoma patient, areas with longer reaction times or no responses at all can be visualised, reflecting visual-field deficits characteristic of the disease.[10,43] The colour scale should be chosen based on the specific question being addressed. Here, the individual visual fields were emphasised. The colour scale was based on the 10th–90th interquartile range of the reaction times divided into five equal steps. A common colour scale should be used for direct comparisons across participants to facilitate quantitative assessments and to avoid misinterpretation of colour differences. Applying the glaucoma participant's colour scale to the healthy participant would make all reaction times appear fast for the healthy participant, highlighting the large differences between the two participants while obscuring small differences within the healthy visual field.

The histograms (Figure 3c,e) of the pooled reaction times across all locations and repetitions demonstrate the skewness of the distributions towards longer reaction times. For the healthy participant, the mean and median were 280 ms and 262 ms, respectively, which do not align well with the mode of the distribution at 242 ms. For the participant with glaucoma, the deviation of the mean (440 ms) was even more pronounced, while, as expected, the median (405 ms) was closer to the mode at 373 ms.

To facilitate visual inspection of deviations from normality, normal probability plots were used (Figure 3d,f). For the healthy participant, deviations from normality are apparent as the reaction times are curvilinear and do not follow the normality line (Figure 3d). Similarly, the deviation from normality is also present in the pooled reaction-time distribution of the participant with glaucoma (Figure 3f). The data deviate from the reference line and are curvilinear. These observations in both example participants imply that at least two independent processes are mixed in the pooled reaction-time distribution. The processes may be linked to distinct areas in the visual field. For participant 3, slow responses were noticeable in the inferior visual field (Figure 3a), while for participant 10, a glaucomatous region in the superior field with slow reaction times was evident (Figure 3b).

Further, it is demonstrated that the promptness distribution pooled across different stimulus conditions, that is, locations in the visual-field task, follows normality. Figure 3 shows the histograms (Figure 3g,i) and probit plots (Figure 3h,j) for the pooled promptness distributions of the two example participants.

For the healthy participant, the promptness histogram (Figure 3g) shows a more symmetric distribution compared to the raw reaction-time histogram (Figure 3c). The reciprobit plot (Figure 3h) demonstrates that the promptness data align well with the straight line, indicating normality. Similarly, for the participant with glaucoma, improvements in distribution symmetry (Figure 3i) and normality (Figure 3j) are observed. The promptness transformation effectively normalises the data for both participants and justifies the use of pooled promptness for further statistical analysis.

As described in the Methods section, to obtain the mean and standard deviation of the promptness distribution, a line was fitted (Figure 3k,l solid black line) to the reciprobit-transformed data within the 25th and 75th percentiles of the distribution (black markers). For the healthy participant, the fit yielded $\mu_{RT} = 262$ ms and $\sigma_{RT} = 50$ ms, compared with $\mu_{RT} = 405$ ms and $\sigma_{RT} = 94$ ms for the participant with glaucoma. The obtained fitted mean reaction times are identical to the medians obtained from the reaction time distributions. For the healthy participant, fast mean reaction times with low variability indicate efficient and consistent visual responses. For the glaucoma patient, slow mean reaction times, with higher variability, reflect the compromised visual field.

Example reciprobit analyses

Figure 4 presents visual-field reaction-time maps and corresponding reciprobit plots of reaction times for one healthy participant (P6) and three participants with glaucoma (P9, P14 and P10) under the 74% contrast viewing condition with the left eye. Each row corresponds to an individual participant. The visual-field maps in the left column follow the same conventions as used in Figure 3a,b, with the addition of light grey circles in the background of locations with less than four repetitions that were excluded from the

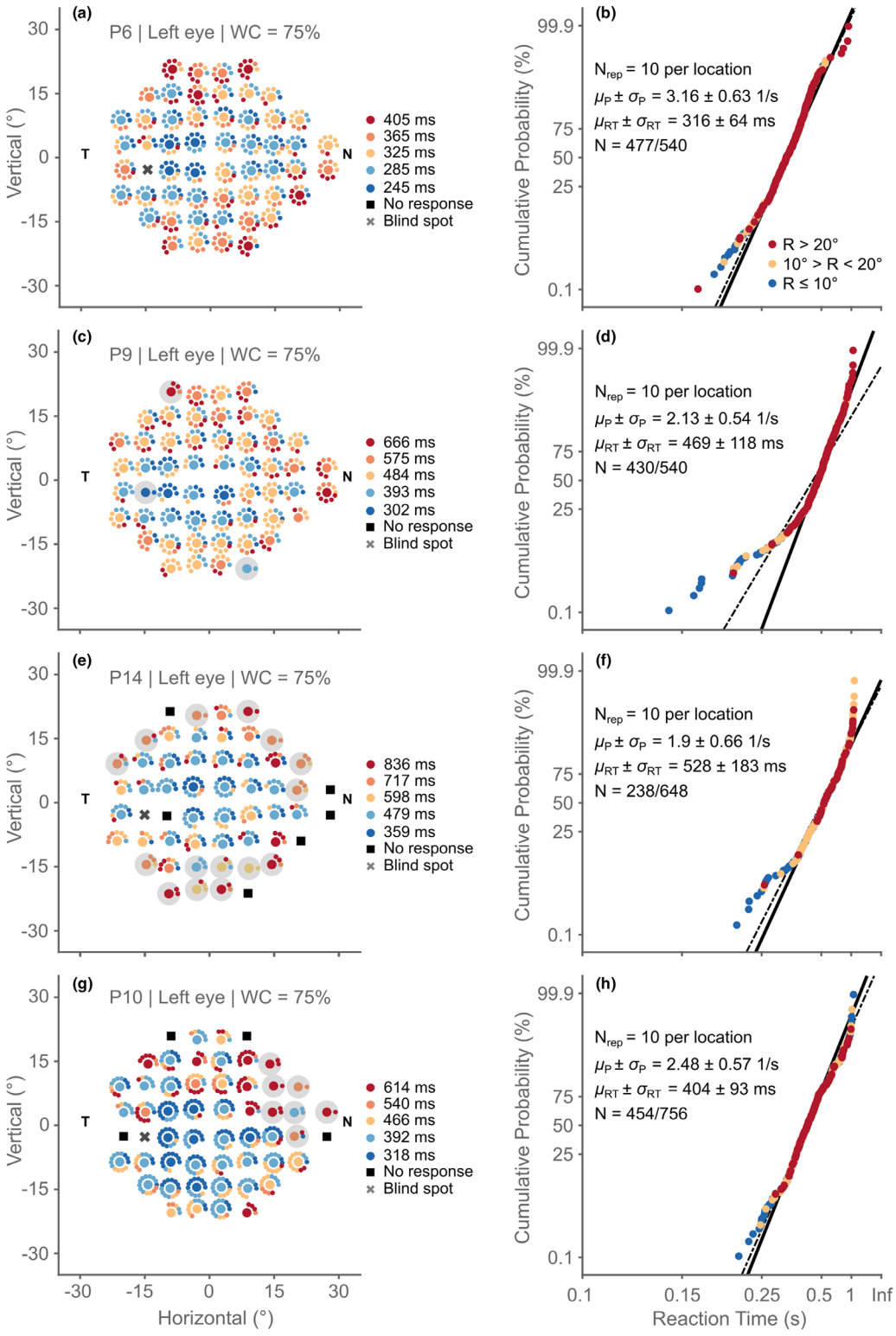

FIGURE 4 Spatial distribution and cumulative distribution of reaction times across the visual field for four participants (P6, P9, P14 and P10) with the left eye and 74% Weber contrast (WC). Left column: Visual field maps (a, c, e, g) show reaction times at all tested target locations. Colours indicate reaction time with cooler colours (blue) representing faster reaction times and warmer colours (red) representing slower reaction times. The black square and grey 'X' indicate locations that did not elicit a goal-directed saccade and the blind spot, respectively. Light grey circles highlight locations with less than four repetitions. Note that the colour scale is not normalised across participants. Right column: Promptness reciprobit plots for each participant (b, d, f, h). Cumulative probability (%) is plotted against promptness (abscissa labels converted to reaction time), showing a linear trend consistent with a normal distribution of promptness. Individual promptness values are colour coded according to target eccentricity with cooler colours indicating central locations and warmer colours peripheral locations. Dashed line = reference normal distribution; Solid black line = linear fit through 25th and 75th percentiles of the data. N = nasal; T = temporal.

error analysis (see Method's section: Parameter-estimation error). Note that the colour scale is not normalised across participants to provide a detailed view of their visual field.

The reaction-time maps reveal spatial variability across the visual field, with peripheral locations generally exhibiting slower reaction times (warmer colours) compared to more central locations (cooler colours). This pattern aligns with known characteristics of visual processing.[26–31] Visual-field loss in glaucoma starts in the periphery and if the disease is left untreated, it progresses centrally.[44,45] This is apparent for participants with glaucoma (Figure 4c,e,g) in that the fastest (central) and slowest (peripheral) reaction times could differ by more than 300 ms compared with 60 ms for the healthy participant of a similar age (Figure 4a). Several peripheral locations did not elicit saccades (filled black squares) for participants 14 (Figure 4e) and 10 (Figure 4g), suggesting full loss of function at these locations. Additionally, the percentage of seen targets at peripheral locations could be well below 50% at affected peripheral locations. This was especially pronounced for participant 13 (Figure 4e). Participant 9 made one goal-directed saccade towards the target presented at the blind spot in one block with two repetitions. A small deviation in the participant's position during testing may have resulted in a slight misalignment during this block. Since no effect of this misalignment was found on the error analysis (see below), no correction was applied for the misalignment and the data from this block were applied in the analysis.

In the right column of Figure 4, reciprobit plots, similar to those in Figure 3k,l, are shown but individual reaction times are colour coded according to target eccentricity (three bins). The reciprobit plots demonstrated that the cumulative distribution of promptness pooled across all locations and repetitions for each participant approximately followed a normal distribution. Adherence to normality was pronounced for participants 6 and 10, while the distributions for participants 9 and 14 deviated from normality. Deviations were due to faster responses at central locations (blue data points). The ratio between fast (cooler colours in the reaction-time map) and slow (warmer colours in the reaction-time map) may be an indicator of deviation from normality. For instance, for participant 9 with the largest deviation from normality, slow responses dominated with only 28% of the responses being fast (RT ≤ 393 ms). In the other participants, fast responses made up at least 40% of all responses (P6: RT ≤ 285 ms; P14: RT ≤ 479 ms) and could even reach 51% for participant 10 (RT ≤ 392 ms), who had the smallest deviation from normality. On a population level across participants and eyes, the correlation between percentage fast responses (RT ≤ 10th percentile plus 25% of the 25th–75th interquartile range) and the quality of the reciprobit fit (mean-squared error and coefficient of determination) was moderate for the 74%-contrast condition (MSE: $R^2 = 0.48$, $p = 0.001$; CoD: $R^2 = 0.51$, $p = 0.001$) and not significant with 155% contrast (MSE: $R^2 = 0.33$, $p = 0.03$; CoD: $R^2 = 0.21$, $p = 0.17$).

The fitted means and standard deviations demonstrated that the healthy participant (Figure 4b) had the fastest reaction times ($\mu_{RT} = 316$ ms; $\mu_P = 3.16$ 1/s) with the least variability ($\sigma_{RT} = 64$ ms; $\sigma_P = 0.63$ 1/s). Participant 10 (Figure 4h) had the fastest ($\mu_{RT} = 403$ ms; $\mu_P = 2.18$ 1/s) and least variable ($\sigma_{RT} = 92$ ms; $\sigma_P = 0.57$ 1/s) reaction times across the three participants with glaucoma. Participant 14 (Figure 4f) was the slowest ($\mu_{RT} = 504$ ms; $\mu_P = 1.98$ 1/s) and most variable ($\sigma_{RT} = 155$ ms; $\sigma_P = 0.61$ 1/s), while participant 9 (Figure 4d) fell in between the two other participants with glaucoma with respect to reaction-time mean ($\mu_{RT} = 466$ ms; $\mu_P = 2.14$ 1/s) and standard deviation ($\sigma_{RT} = 116$ ms; $\sigma_P = 0.53$ 1/s). All fits captured the central tendency appropriately and aligned well with the data.

The observed linear trend suggests that this method of transforming reaction times to promptness produces or approximates normal distributions. The slight deviations from linearity at the extremes reflect the inhomogeneity of the visual field and may be accounted for by focusing the analysis on, for example, central or peripheral locations separately. Even with deviations from normality, limiting the fit to the 25th and 75th percentiles results in a robust estimate of the central tendency that provides a two-parameter summary of the visual-field function.

Parameter estimation error as a function of repetition count per location

Figure 5 illustrates the impact of repetition count per location on estimation errors for reaction-time parameters across the same four participants shown in Figure 4 (P6, P9, P14 and P10) for the left eye and target contrast of 74%. The figure is organised into two columns for each participant: the left column shows reciprobit plots constructed from distributions based on one repetition randomly drawn per location; the right column presents the estimation-error distributions for the reaction-time mean (μ_{RT}) and standard deviation (σ_{RT}) as a function of repetition count (See Method's section: Parameter-estimation error).

The reciprobit plots in the left column can be compared directly with the reciprobit plots shown in Figure 4, which are based on the full number of repetitions. They confirm that the promptness distributions based on a limited data set approximate normality for all participants. This makes it possible to use the mean and standard deviation as summary statistics, even with a limited number of repetitions. The same trends with regard to mean and standard deviation for the four example participants observed with the full data set (Figure 4) were also present in the distributions based on the dataset limited to one repetition per location (Figure 5). The parameter estimates with one repetition per location could deviate marginally from the parameters obtained with the full set.

The estimate of mean reaction time (μ_{RT}) deviated slightly across all participants, with participants 6 and 9 having the lowest deviation (3 and 8 ms) and participants 10 and 14 having a slightly larger deviation (both 14 ms). The same held true for the estimates of reaction-time standard deviation (σ_{RT}), which were low for participants

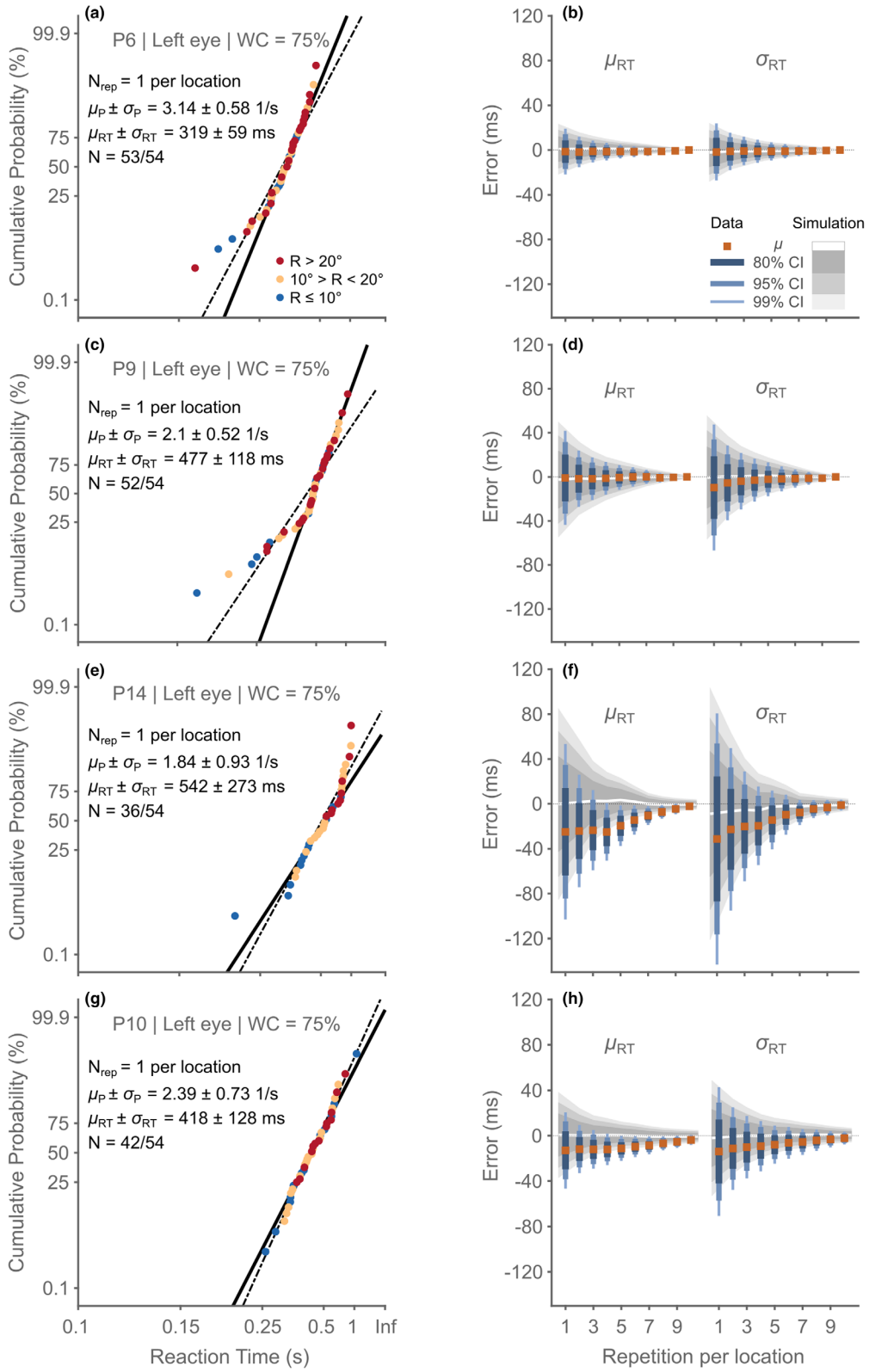

FIGURE 5 Impact of repetition count on estimation errors for reaction-time (RT) parameters across four participants (a,b: P6, c,d: P9, e,f: P14 and g,h: P10) under left-eye and 74% Weber contrast (WC) viewing conditions. Left column: Reciprobit plots for distributions based on randomly drawing one repetition from all available repetitions per location. Conventions as in Figure 3. Right column: Estimation errors for the mean (μ_{RT}) and standard deviation (σ_{RT}) of reaction times as a function of the number of repetitions per location (1 to 10). Each density plot shows the mean error (orange square), 80%/95%/99% confidence interval (CI; vertical lines in hues of blue) of the data and simulations based on the data (white line = mean; grey patches = CI's).

6 (5 ms) and 9 (0 ms) and slightly higher for participant 10 (35 ms). For participant 14, the deviation between the two estimates of reaction-time standard deviation was the largest (90 ms), which is a result of that participant's large standard deviation (σ_{RT} = 183 ms), obtained with the full number of repetitions. The reciprobit plots obtained from the limited dataset per participant, that is, one repetition randomly selected per location, confirm that it is feasible to estimate reaction-time distribution parameters by pooling across locations. With this analysis approach, it is possible to obtain a general estimate of a participant's performance, for example, across the visual field.

Next, the influence of repetition count on the parameter estimates was examined. Specifically, the deviation between the estimates of the mean ($\boldsymbol{E}_{\mu}$) and standard deviation ($\boldsymbol{E}_{\sigma}$) obtained was compared with the full dataset based on all available repetitions, with the estimates obtained with a limited number of repetitions. The right column of Figure 5 displays error distributions (in ms) for mean reaction time (μ_{RT}) and standard deviation (σ_{RT}) as a function of repetition count per location, ranging from 1 to 10 repetitions. Each plot includes the mean error (orange square) and 80%/95%/99% confidence intervals (vertical lines in hues of blue). Additionally, the white line and the grey patches indicate, respectively, the mean error and the 80%/95%/99% confidence intervals of simulated normal distributions based on the parameter estimates obtained from the empirical data (see Method's section: Parameter-estimation error). The simulations provide a reference for the case that the underlying distributions are all normal and avoid sampling bias that may be present in the empirical distributions, that is, a limited number of repetitions to draw from.

With fewer repetitions, the estimation error for both μ_{RT} and σ_{RT} shows greater variability, with broader error distributions and increased error magnitudes for all participants. As the number of repetitions per location increases, the error distributions narrow, reflecting increased estimation stability. Error variability and magnitude are generally larger for the standard-deviation estimate since the slope is more susceptible to small differences in sample composition compared to the 50% probability point. Interestingly, both parameter estimates tend to be biased towards overestimation (negative errors). Parameter overestimation may lead to effect size inflation. Therefore, a careful examination of condition pooling on parameter estimation is necessary that can be informed by the proposed reciprobit analysis. In a clinical context, overestimation may be beneficial as it will lead to a false positive diagnosis rather than a false negative one. Since for clinical anamnesis, multiple diagnostics will be considered together in the patient's evaluation, false positives may be preferable to prompt further investigation. Parameter overestimation is especially prominent for participants 14 (Figure 5f) and 10 (Figure 5h) with late-stage glaucoma. For participant 9 with moderate glaucoma (Figure 5d) and the healthy participant (Figure 5b), mean error magnitudes with all repetitions are close to zero, indicating adequate estimation.

Estimation error is correlated with response variability

Figure 6 displays the relationship between reaction-time standard deviation (σ_{RT}) and mean errors of the mean estimate (left column) and the standard-deviation estimate (right column) based on one repetition per location for both contrasts, eyes and participant groups. Individual participants contributed four data points (two contrasts and two eyes). Each subplot represents data from a different group: healthy participants (Figure 6a,b), glaucoma participants (Figure 6c,d) and a combined view of healthy and glaucoma participants (Figure 6e,f). Data points are colour-coded, with each colour representing a different participant and group.

A negative trend is apparent in all panels, indicating that higher variability in reaction times (σ_{RT}) is associated with greater (more negative) mean error in the parameter estimate. Regression lines fitted to the data in each panel are accompanied by model statistics, including the regression equation, 95% highest density interval (HDI) for the slope, coefficient of determination (R^2) and p-value. All fits were significant except for the fit describing the error of the standard-deviation estimate for the participants with glaucoma (Figure 6d). The linear model described about 50% of the variability for the mean estimate (highest: 56% combined group), indicating a moderate correlation. For all three groups, an increase of σ_{RT} by 20 ms led to an increase of about 1 ms in estimation error of mean reaction time.

For the standard-deviation error, the linear model described 63% of the variability observed in the healthy group, indicative of good predictive power. The slope of −0.04 [−0.05 to 0.04] (Figure 6b) was similar to that observed for the mean estimate (Figure 6a,c,e). For the combined group (Figure 6f), the R^2 was 0.44, indicating a relatively weak fit of the model to the data. Several data points contributed by participants 14 and 13 limited the model's predictive power. Removing these data increased the R^2 to 0.59 without changing the slope estimate; an increase of σ_{RT} by 20 ms led to an increase in error of about 1.2 ms in estimation error of reaction-time standard deviation. Excluding the extreme data points for the glaucoma group resulted in a significant fit ($p = 4 \times 10^{-5}$), with moderate correlation (R^2 = 0.57) and an increase of error by 1.2 ms for each 20 ms of σ_{RT}.

The weak to moderate correlations for both the mean and the standard deviation estimates indicated that other factors not included in a simple linear model influence the relation between error and σ_{RT}. While the correlations reported here are useful as a rule of thumb, for participants with (severe) glaucoma, this suggests that a thorough characterisation with sufficient repetitions will be needed for an accurate estimate of overall reaction time across the visual field. However, note that given the pronounced reaction time deficits in severe glaucoma (2–3 times slower than healthy participants), detection of the disease will not be hampered by the estimation errors reported here. Less severe cases of glaucoma most likely will fall in between the healthy participants and those with glaucoma shown here.

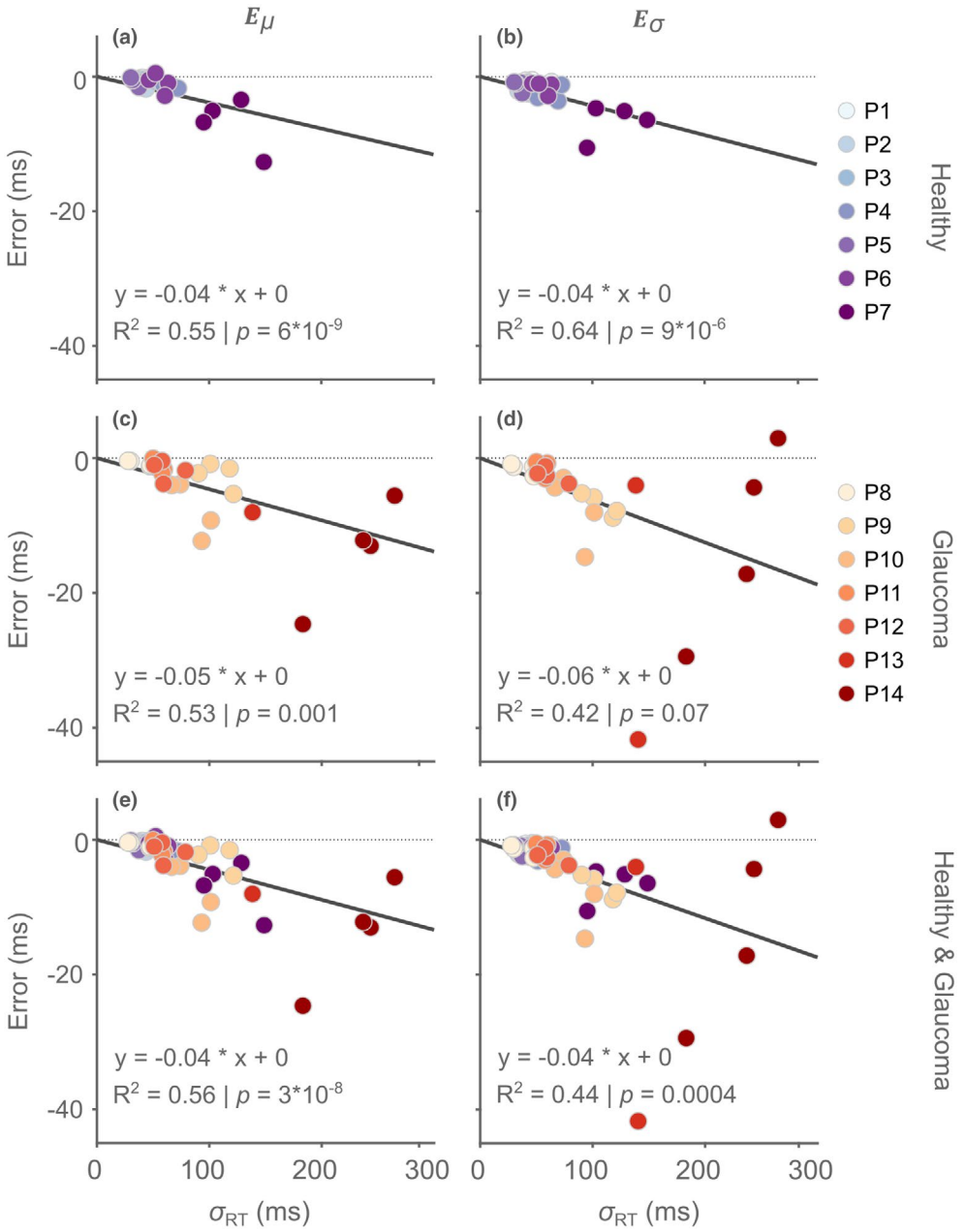

FIGURE 6 Relationship between reaction-time variability (σ, in ms) and estimation error in reaction-time parameter estimation (in ms; left column: Mean, μ_{RT}; right column: Standard deviation, σ_{RT}) based on one repetition per location for healthy participants (a, b), glaucoma participants (c, d) and combined groups (e, f). Data points represent individual participants across conditions (contrasts and eyes), with colours distinguishing participants and subgroups. Regression lines (black line) with 95% highest density intervals (HDIs; grey patch) highlight a negative trend in all panels, indicating that increased variability in reaction times corresponds to greater (negative) mean error in parameter estimates. Model statistics are provided for each regression line, including slope, HDI, coefficient of determination (R^2) and p-value.

Limiting the conditions for pooling decreases estimation error

Pooled promptness distributions for participants with glaucoma could deviate from normality due to inhomogeneities across their visual field (Figure 4d,f). Large deviations may impact parameter estimation (Figure 5). Estimation errors can be decreased by increasing the normality of the pooled promptness distribution. This study examined if limiting the range of pooled conditions aids in the normalisation of the promptness distribution. For the visual-field measurements described here, this translates to restricting the included target locations. To demonstrate this approach, reciprobit plots were constructed including only targets with eccentricities greater than 15° (Figure 7) and performing the parameter estimation error analysis (Figure 8).

Figure 7 displays reciprobit plots for the same participants shown in Figures 4 and 5 constructed using peripheral target locations ($R > 15°$) for the left eye and 74%-contrast

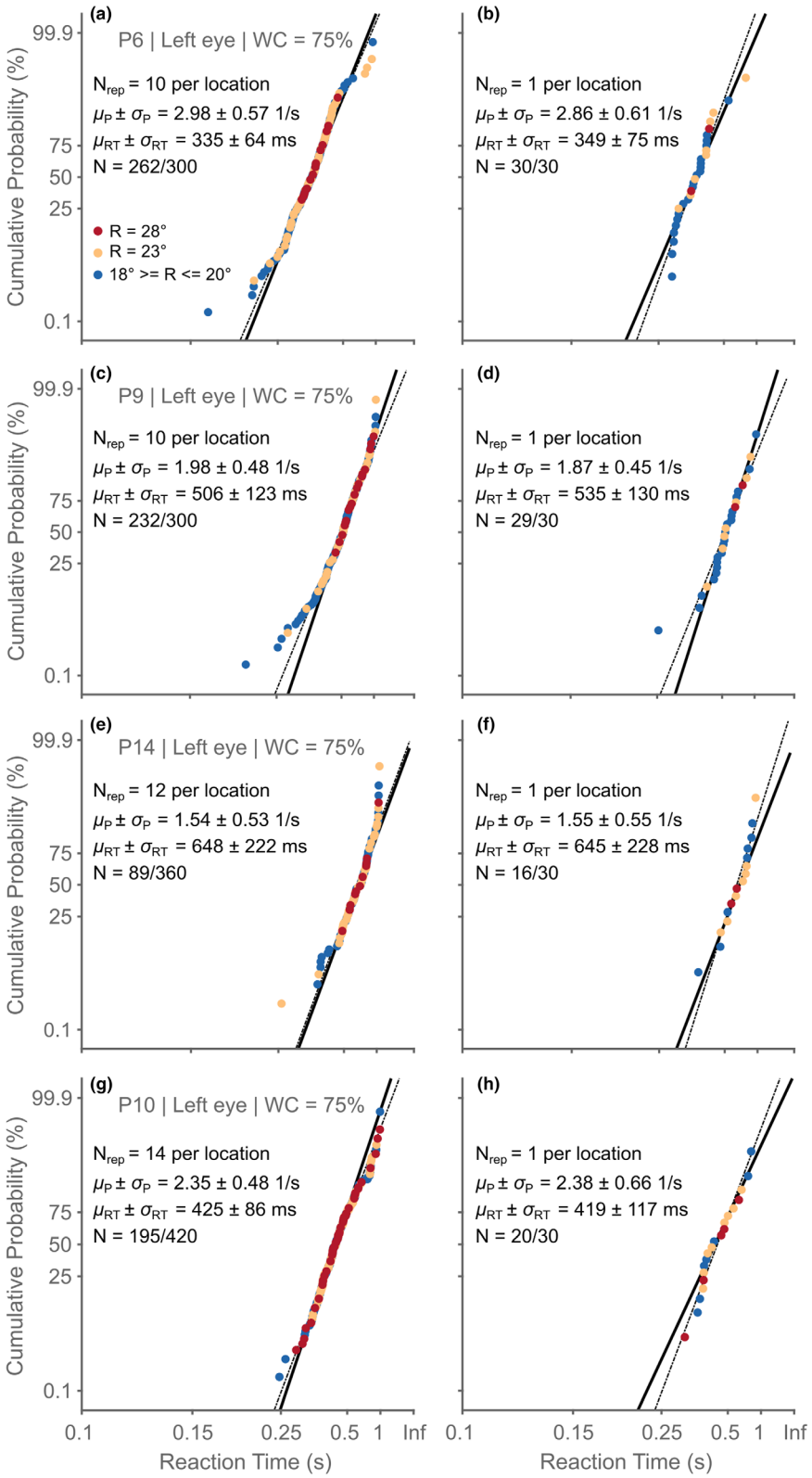

FIGURE 7 Reciprobit plots for target eccentricities >15° for four participants (a,b: P6, c,d: P9, e,f: P14 and g,h: P10) under left-eye and 74% Weber contrast (WC) viewing conditions. Left column: All available repetitions per location are included for the construction of the reciprobit plot. Right column: One repetition per location is randomly drawn and included in the plot. Individual promptness values are colour-coded according to target eccentricity. Dashed line = reference normal distribution; Solid black line = linear fit through 25th and 75th percentiles of the data.

condition. Data points are colour-coded by target eccentricity. The inclusion of peripheral rather than central locations was motivated by the patterns of glaucoma progression.[44–46] The left column of Figure 7 depicts reciprobit plots constructed with all available repetitions (compare with Figure 4 right column), while in the right column, only one repetition per location was randomly selected and included (compare with Figure 5 left column).

All four participants' data closely follow the reference normality line (dashed line), both for all repetitions (left column) and for one repetition per location (right column). For participants 9 and 14 with glaucoma, the deviations from normality were reduced with the limited range of targets, unlike the reciprobit plots across the full range of targets (Figure 4d,f). For participant 9, deviations were most pronounced due to targets with eccentricities $18° \leq R \leq 20°$ (Figure 7c). In this case, reducing the included target locations to eccentricities greater than 20° could further normalise the promptness distribution. Note that for the experimental design adopted here, this would come at the expense of reducing the available number of targets, that is, with one repetition per location, down from 30 to 10 locations. Such a large reduction could potentially impact parameter estimation. Accordingly, careful examination of the reciprobit plots and weighing of the pooling scheme is generally advisable.

Comparing across participants, the same individual differences and trends evident in reaction times observed with the full range of target locations were also noticeable when restricting the target range. Participant 14 with glaucoma (Figure 7e) had the slowest mean reaction time (μ_{RT} = 648 ms; μ_P = 1.54 1/s) and largest standard deviation (σ_{RT} = 222 ms; σ_P = 0.53 1/s) followed by participant 9 with glaucoma (μ_{RT} = 506 ms, σ_{RT} = 123 ms; μ_P = 1.98 1/s, σ_P = 0.48 1/s; Figure 7c) and participant 10 with glaucoma (μ_{RT} = 425 ms, σ_{RT} = 86 ms; μ_P = 2.35 1/s, σ_P = 0.48 1/s; Figure 7g). As with the full range, healthy participant 6 (Figure 7a) had the fastest mean reaction times (μ_{RT} = 335 ms; μ_P = 2.98 1/s) and the least variability (σ_{RT} = 64 ms; σ_P = 0.57 1/s). The observed robustness of the reaction time parameter trends to different pooling strategies is promising, for example, for the refinement of glaucoma detection paradigms.

As with the promptness distributions based on the full target range, parameter estimates with one repetition per location deviated slightly from the parameters obtained with all repetitions. The estimate of mean reaction time (μ_{RT}) deviated slightly for participants 6 (5 ms), 9 (3 ms) and 14 (2 ms), while the difference for the shown sample distribution was larger for participant 10 (27 ms). The estimate of reaction-time standard deviation (σ_{RT}) for participants 9 and 14 was small, 1 ms and 2 ms, respectively. For participant 10, the deviation between the two estimates of reaction-time standard deviation was the largest (29 ms), while moderate (14 ms) for healthy participant 6. Increased deviations are expected given the reduced number of available responses with the limited target range and only one repetition per location (max. 30 samples).

The parameter-estimation errors obtained using both the full target range and the limited target range ($R > 15°$) were compared across all participants and conditions. It was expected that for healthy participants, reducing the target range would not impact the quality of the μ_{RT} estimate. In these participants, promptness distributions for both the full and the limited ranges closely followed normality, indicating that μ_{RT} estimates should be accurate. However, the σ_{RT} estimate may be susceptible to the reduced number of available samples, that is, similar or larger error. In participants with glaucoma, parameter-estimation errors should be smaller with the limited target range. In these participants, limiting the range for pooling will result in promptness distributions that will closely follow normality.

Figure 8 shows the correlation between estimation errors calculated from a limited range of target eccentricities ($R > 15°$) and errors derived from the full target range with one repetition per location for both reaction-time mean (μ_{RT}, left column) and reaction-time standard deviation (σ_{RT}, right column). Each row represents a different participant grouping: the top row includes healthy participants, the middle row participants with glaucoma and the bottom row all participants. In the scatter plots, each marker represents the bootstrapped mean error, with distinct colours used to differentiate individual participants. Each participant contributed four data points (two contrasts and two eyes). In each panel, regression lines fitted to the data (black line) and 95% highest density intervals (grey patch) are accompanied by model statistics, including the regression equation, coefficient of determination (R^2) and p-value. For the slope, values close to or greater than 1, respectively, indicate that the errors obtained with the limited and full target ranges are similar to each other and that the error for the limited target range is larger than the full range error. Values smaller than 1 indicate that the error obtained with the limited range is smaller than the error obtained with the full target range.

For the healthy participants, errors clustered close to the unity line for both μ_{RT} (Figure 8a) and σ_{RT} (Figure 8b). The fit for μ_{RT} was not significant, whereas the fit for σ_{RT} was significant and the correlation was high (R^2 = 0.84). The slope was close to 1 (σ_{RT}: m = 1.15 [0.98 1.32]). For both μ_{RT} and σ_{RT}, errors of participant 7 differed from those of the other participants. For μ_{RT} errors, the limited range resulted in smaller errors across all four conditions. For σ_{RT}, participant 7 had the largest errors among all seven healthy participants. Participant 7 was the oldest in our sample of healthy participants (64 years) and, while not clinically diagnosed with glaucoma, is the sister of participants 13 and 14, both clinically diagnosed with glaucoma (Table 1). Overall, the results confirmed the hypotheses that reducing the target range does not affect μ_{RT} errors but may result in increased σ_{RT} errors due to a reduced number of samples used in the reciprobit fit.

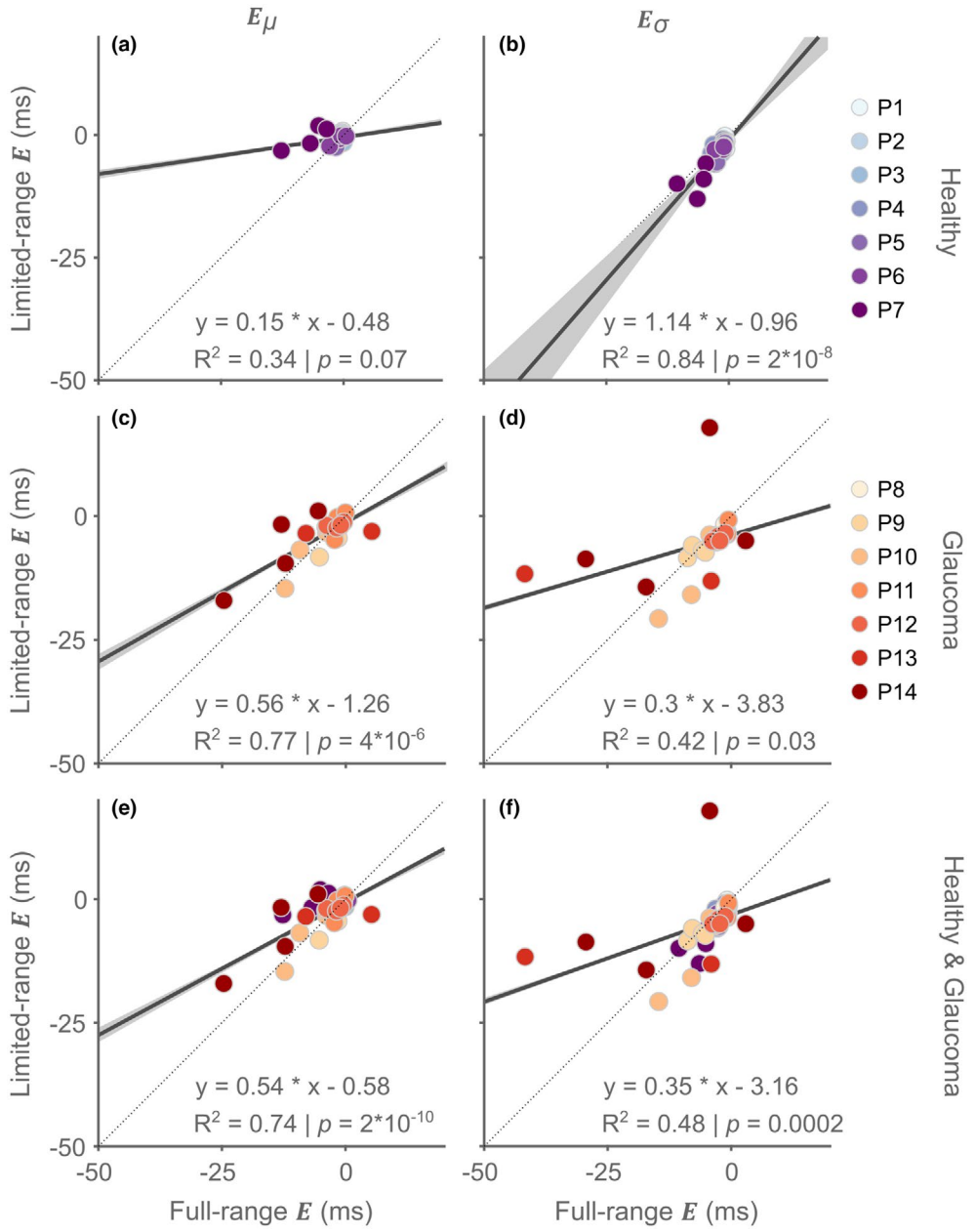

FIGURE 8 Comparison of estimation errors, ***E***, from a limited range of target eccentricities (>15°) with errors from the full range of eccentricities for reaction-time mean (μ_{RT}, left column) and standard deviation (σ_{RT}, right column) parameters across different participant groupings: Healthy participants (a, b), glaucoma (c, d) and all participants (e, f). Each participant contributed four points (two contrasts and two eyes). Regression lines with 95% highest density intervals (HDIs) are included, along with model parameters: Slope, HDI, R^2 and *p*-value. Parameter estimates based on one repetition per location.

For the participants with glaucoma (Figure 8c,d), a significant positive correlation was observed for mean reaction time ($R^2 = 0.77$), and the slope of the regression line was smaller than 1 (μ_{RT}: m = 0.56 [0.5 0.62]) indicating that the error with the limited target range was smaller than that obtained with the full range (Figure 8c). The fit was not significant ($p = 0.03$) for the standard-deviation estimate and was driven by two data points from participants 13 and 14 (Figure 8d). Most of the data were distributed close to the unity line or fell below the line. Removing the two extreme points from participants 13 and 14 resulted in a significant fit ($p = 7 \times 10^{-8}$; $R^2 = 0.9$) with a slope slightly larger than 1 ($m = 1.18$ [1.06 1.32]). While the fit for the combined group was significant ($p = 0.0002$), the correlation was weak ($R^2 = 0.48$) due to the two data points of participants 13 and 14 (Figure 8f). Removing these two points resulted in a strong correlation increase ($R^2 = 0.89$; $p = 4 \times 10^{-17}$) and a slope slightly larger than 1 ($m = 1.18$ [1.07 1.28]). This suggests that the standard deviation, as expected, is more difficult to estimate from the reciprobit fit compared to the mean and benefits from a well-sampled distribution.

DISCUSSION

This study introduced an efficient method for analysing reaction-time data in EMP based on promptness distributions pooled across visual-field locations. By using promptness as the primary metric and constructing reciprobit plots, it was demonstrated that key distributional parameters (mean and standard deviation of promptness) can be estimated with minimal repetitions per condition, that is, location, supporting the feasibility of this approach for clinical applications. At least 3–5 repetitions per location are needed to achieve reliable estimates of μ_{RT} and σ_{RT}, as additional repetitions produce diminishing returns on error reduction. This result has practical implications for experimental design, especially in clinical settings, where reducing the number of trials can mitigate participant fatigue without significantly compromising the accuracy of reaction-time parameter estimates.

Rather than proposing a new transformation per se, the goal was to validate and operationalise the promptness metric within the specific context of EMP. It is shown that this transformation enables efficient pooling and comparison across sparse spatial data, potentially offering new avenues for clinical visual-field screening and longitudinal tracking.

Pooled promptness distributions: Normality and practical considerations

A central issue in the analysis is whether pooled promptness distributions approximate normality sufficiently for reliable parameter estimation. Because reaction times vary across the visual field due to eccentricity[26–31] and potential visual deficits,[10] the pooled distribution is theoretically a mixture rather than a single normal distribution. As shown in Figures 4 and 7, deviations from normality may emerge when pooling across locations with highly divergent response properties. In this context, reciprobit plots offer a diagnostic tool for evaluating distribution shape and guiding the selection of appropriate target-grouping strategies. Analysts may, for example, choose to exclude central locations or stratify by eccentricity to improve the robustness of parameter estimation. It is emphasised that this flexibility is a strength of the approach, allowing it to be adapted to individual datasets or clinical needs. These findings suggest that in many cases, the deviations from normality are minor and do not substantially impact parameter estimates.

For participants with an intact visual field, parameter estimation was straightforward. Pooling promptness across target locations resulted in normal distributions despite the well-known reaction-time gradient across the visual field. Even with only one repetition per location, which resulted in a total of 53 samples, pooled promptness distributions remained normal and estimation errors (~0 ms) and error distribution confidence intervals (99% CI < 40 ms) for the mean and standard deviation were small, relative to the parameters obtained with all available repetitions. These findings suggest that promptness pooling can improve data robustness, streamline data collection and enable more generalised assessments, especially when sample sizes are limited.

In participants with glaucoma, the difference between central and peripheral reaction times was markedly larger than in healthy participants, consistent with the progression of visual-field loss typically observed in glaucoma.[44–46] Pooled promptness distributions of individual participants could deviate from normality, increasing parameter-estimation errors (~20 ms) and variability (error 99% CI ~200 ms) when reducing the number of repetitions per target location to one. Deviations from normality were associated with a lower proportion of fast responses, that is, a skew towards slower reaction times as visual-field degradation increases. The promptness data of participants with glaucoma was normalised by altering the pooling scheme to only include peripheral locations ($R > 15°$). As a result, estimation error, that is, estimate robustness, especially for the mean decreased, but estimate variability increased due to the reduced number of samples. As demonstrated in Figure 8, this trade-off may lead to increased estimation error, depending on the number of included locations and the participant's field characteristics. Therefore, limiting the spatial range should be considered a flexible, data-driven strategy that can enhance robustness in some cases, but may not improve estimation precision universally. Promptness transformation and pooling simplifies parameter estimation of reaction-time distributions; however, the underlying assumption that promptness is normally distributed across the pooled visual-field locations needs to be validated. That is, the pooling scheme should be tailored to the specific application taking stimuli, task design and (clinical) populations into account. The reciprobit plot facilitates this analysis. If pooling is done correctly, the proposed analysis method offers a stable estimate of central tendency and dispersion. Future large-scale studies should quantify further the conditions under which this assumption holds and explore methods to correct for potential skewness in extreme cases.

Overall, these results suggest that the promptness-based approach, visualised in reciprobit plots, effectively characterises the distribution of reaction times across the visual field. The consistency of these trends across participants supports the robustness of the method in capturing spatial and individual variability, offering a practical solution for clinical assessments requiring efficiency in data acquisition and interpretation. Reciprobit plots provide a framework to evaluate the appropriateness of the pooling strategy and the stability of derived distributional parameters.

Clinical relevance of promptness metrics

A major advantage of the proposed method is that it allows estimation of central tendency and variability of

reaction times without requiring many repetitions per location. This efficiency is critical in clinical applications, where patient fatigue limits test duration.[10,12,47] Despite the practicality of using fewer repetitions, the precision of the mean and standard deviation estimates improved as the repetition count increased, with error distributions narrowing and error magnitudes decreasing. While single-repetition estimates can provide a general overview, three to five repetitions per location will result in more reliable parameter estimates at the expense of longer measurement times. Beyond this threshold, additional repetitions offer diminishing returns in terms of error reduction, which is particularly relevant for designing efficient clinical protocols.

As to the question of how these promptness-based metrics should be used clinically, we propose that the mean and standard deviation of promptness could serve as summary indices akin to mean deviation (MD) in standard perimetry.[43] While the present findings demonstrate that promptness-based parameters (μ_{RT} and σ_{RT}) can be estimated reliably even from sparse data and show promise as compact summary measures of visual field function, it should be emphasised that this study was not designed to evaluate clinical diagnostic performance. Direct comparisons with standard perimetric indices such as MD, or assessments of diagnostic sensitivity and specificity, were beyond the scope of the present work. Rather, the goal here was to establish a statistically robust framework that can support such future evaluations. Systematic validation of promptness-based indices in a clinical setting—including their relationship with conventional metrics and their utility in disease classification—remains an important next step. Future studies should compare the diagnostic power of these promptness-based indices to established perimetric metrics and determine whether they provide added sensitivity to functional deficits.

Limitations and future directions

While pooled promptness distributions technically represent mixtures due to location-specific latency effects, this empirical analysis suggests that they closely approximate normality under typical perimetric conditions. This justifies the use of parametric models for practical purposes, though this approximation may not hold in more heterogeneous populations or stimulus regimes.

Pooling data across conditions enhances efficiency. However, it may obscure condition-specific, that is, location-specific, effects. In clinical EMP applications, it will be crucial to balance the need for data reduction with the retention of spatially relevant diagnostic information.[44] Additionally, further validation in larger patient cohorts is needed to assess the robustness of promptness-based indices across different severities and patterns of visual impairment.

This use of promptness as a descriptive measure is intended for contexts where theoretical model fitting is infeasible or unnecessary—such as low-trial perimetric tests in clinical settings. We do not position promptness as a substitute for process models, for example, drift-diffusion, but as a practical alternative in high-throughput or sparse-sampling scenarios.

CONCLUSIONS

In summary, these findings support the use of pooled promptness distributions as a practical approach to reaction-time analysis in EMP. Future work should refine these metrics and validate their clinical utility for detecting and monitoring visual-field deficits.

AUTHOR CONTRIBUTIONS

Ashwini Venkat Reddy Chanakya: Data curation (supporting); formal analysis (equal); investigation (equal); software (equal); validation (equal); visualization (equal); writing – original draft (lead); writing – review and editing (equal). **Peter Bremen:** Conceptualization (lead); data curation (lead); formal analysis (equal); funding acquisition (lead); investigation (equal); methodology (lead); project administration (lead); resources (lead); software (equal); supervision (lead); validation (equal); visualization (equal); writing – original draft (supporting); writing – review and editing (equal).

ACKNOWLEDGEMENTS

This work was supported by Stichting Lijf en Leven, Krimpen aan den Ijssel (74_P.Bremen) (PB), Oogfonds (2022-12) (AC) and Erasmus MC Rotterdam (PB). We gratefully acknowledge Dr. Ronnie George and Dr. Johan Pel EngD who provided much appreciated support throughout the study and allowed us to use the Eye-Movement Perimetry setup. We thank Robert Beurskens for invaluable technical assistance and facilitating the Photron reference measurements and Katharina-Inés Janisch for assistance with participant recruitment and pilot photodiode timing measurements.

FUNDING INFORMATION

This work was supported by Stichting Lijf en Leven, Krimpen aan den Ijssel (74_P.Bremen) (PB), Oogfonds (2022-12) (AC) and Erasmus MC Rotterdam (PB).

CONFLICT OF INTEREST STATEMENT

The authors have no relevant financial or non-financial interests to disclose.

DATA AVAILABILITY STATEMENT

The dataset and analysis code are available in the figshare repository, https://figshare.com/s/252433edbd6cdc2d8791.

CONSENT

Informed consent to participate and for publication was obtained from all participants included in the study.

ORCID

Ashwini Venkat Reddy Chanakya https://orcid.org/0000-0002-0151-4578
Peter Bremen https://orcid.org/0000-0003-1709-6224

REFERENCES

1. Posner MI. Orienting of attention. *Q J Exp Psychol*. 1980;32:3–25.
2. Posner MI. Orienting of attention: then and now. *Q J Exp Psychol*. 2016;69:1864–75.
3. Prinzmetal W, McCool C, Park S. Attention: reaction time accuracy reveal different mechanisms. *J Exp Psychol Gen*. 2005;134:73–92.
4. Palmer J, Huk AC, Shadlen MN. The effect of stimulus strength on the speed and accuracy of a perceptual decision. *J Vis*. 2005;5:376–404.
5. Noorani I, Carpenter RHS. The LATER model of reaction time and decision. *Neurosci Biobehav Rev*. 2016;64:229–51.
6. Donders FC. On the speed of mental processes. *Acta Psychol*. 1969;30:412–32.
7. Mansfield RJW. Latency functions in human vision. *Vis Res*. 1973;13:2219–34.
8. Luce RD. Response times: their role in inferring elementary mental organization. New York: Oxford Academic; 1986.
9. Pel JJM, Van Beijsterveld MCM, Thepass G, Van der Steen J. Validity and repeatability of saccadic response times across the visual field in eye movement perimetry. *Transl Vis Sci Technol*. 2013;2:3. https://doi.org/10.1167/tvst.2.7.3
10. Mazumdar D, Kadavath Meethal NS, Panday M, Asokan R, Thepass G, George RJ, et al. Effect of age, sex, stimulus intensity and eccentricity on saccadic reaction time in eye movement perimetry. *Transl Vis Sci Technol*. 2019;8:13. https://doi.org/10.1167/tvst.8.4.13
11. Tatham AJ, Murray IC, McTrusty AD, Cameron LA, Perperidis A, Brash HM, et al. Speed and accuracy of saccades in patients with glaucoma evaluated using an eye tracking perimeter. *BMC Ophthalmol*. 2020;20:259. https://doi.org/10.1186/s12886-020-01528-4
12. Thepass G, Lemij HG, Vermeer KA, van der Steen J, Pel JJM. Slowed saccadic reaction times in seemingly normal parts of glaucomatous visual fields. *Front Med (Lausanne)*. 2021;8:679297. https://doi.org/10.3389/fmed.2021.679297
13. Trope GE, Eizenman M, Coyle E. Eye movement perimetry in glaucoma. *Can J Ophthalmol*. 1989;24:197–9.
14. Kim DE, Eizenman M, Trope GE, Kranemann C. Eye movement perimetry. Proceedings of 17th international conference of the engineering in medicine and biology society. Montreal: IEEE; 1995. p. 1629–30. https://doi.org/10.1109/IEMBS.1995.579863
15. Ulrich R, Miller J. Effects of truncation on reaction time analysis. *J Exp Psychol Gen*. 1994;123:34–80.
16. Ratcliff R, McKoon G. The diffusion decision model: theory and data for two-choice decision tasks. *Neural Comput*. 2008;20:873–922.
17. Whelan R. Effective analysis of reaction time data. *Psychol Rec*. 2008;58:475–82.
18. Ratcliff R. A theory of memory retrieval. *Psychol Rev*. 1978;85:59–108.
19. Gold IJ, Shadlen MN. Neural computations that underlie decisions about sensory stimuli. *Trends Cogn Sci*. 2001;5:10–6.
20. Brown S, Heathcote A. QMLE: fast, robust and efficient estimation of distribution functions based on quantiles. *Behav Res Methods Instrum Comput*. 2003;35:485–92.
21. Forstmann BU, Ratcliff R, Wagenmakers EJ. Sequential sampling models in cognitive neuroscience: advantages, applications and extensions. *Annu Rev Psychol*. 2016;67:641–66.
22. Van Zandt T. How to fit a response time distribution. *Psychon Bull Rev*. 2000;7:424–65.
23. Ratcliff R, Tuerlinckx F. Estimating parameters of the diffusion model: approaches to dealing with contaminant reaction times and parameter variability. *Psychon Bull Rev*. 2002;9:438–81.
24. Ratcliff R. Methods for dealing with reaction time outliers. *Psychon Bull*. 1993;114:510–32.
25. Carpenter RHS, Williams ML. Neural computation of log likelihood in control of saccadic eye movements. *Nature*. 1995;377:59–62.
26. Bartz AE. Eye movement latency, duration and response time as a function of angular displacement. *J Exp Psychol*. 1962;64:318–24.
27. Osaka N. Reaction time as a function of peripheral retinal locus around fovea: effect of stimulus size. *Percept Mot Skills*. 1976;42:603–6.
28. Cohen ME, Ross LE. Saccade latency in children and adults: effects of warning interval and target eccentricity. *J Exp Child Psychol*. 1977;23:539–49.
29. Honda H, Findlay JM. Saccades to targets in three-dimensional space: dependence of saccadic latency on target location. *Percept Psychophys*. 1992;52:167–75.
30. Kalesnykas RP, Hallet PE. Retinal eccentricity and the latency of eye saccades. *Vis Res*. 1994;34:517–31.
31. Greene HH, Brown JM, Dauphin B. When do you look where you look? A visual field asymmetry. *Vis Res*. 2014;102:33–40.
32. Brascamp JW, Naber M. Eye tracking under dichoptic viewing conditions: a practical solution. *Behav Res Methods*. 2017;49:1303–9.
33. Qian CS, Brascamp JW. How to build a dichoptic presentation system that includes an eye tracker. *J Vis Exp*. 2017;6:33. https://doi.org/10.3791/56033
34. Meethal NSK, Mazumdar D, Morshchavka S, Robben J, Van der Steen J, George R, et al. A haploscopic based binocular pupillometer system to quantify the dynamics of direct and consensual pupillary light reflex. *Sci Rep*. 2021;11:21090. https://doi.org/10.1038/s41598-021-00434-z
35. American Academy of Ophthalmology. Automated perimetry. *Ophthalmology*. 1996;103:1144–51.
36. Ottes FP, Van Gisbergen JA, Eggermont JJ. Visuomotor fields of the superior colliculus: a quantitative model. *Vis Res*. 1986;26:857–73.
37. Goossens HHLM, Van Opstal AJ. Dynamic ensemble coding of saccades in the monkey superior colliculus. *J Neurophysiol*. 2006;95:2326–41.
38. Jóhannesson O, Tagu J, Kristjánsson A. Asymmetries of the visual system and their influence on visual performance and oculomotor dynamics. *Eur J Neurosci*. 2018;48:3426–45.
39. Corneil BD, Van Wanrooij MM, Munoz DP, Van Opstal AJ. Auditory-visual interactions subserving goal-directed saccades in a complex scene. *J Neurophysiol*. 2002;88:438–54.
40. Veugen LCE, Van Opstal AJ, Van Wanrooij MM. Reaction time sensitivity to spectrotemporal modulations of sound. *Trends Hear*. 2022;26:23312165221127589. https://doi.org/10.1177/23312165221127589
41. Jensen JLWV. Sur les fonctions convexes et les inégalités entre les valeurs moyennes. *Acta Math*. 1906;30:175–93.
42. Bremen P, Massoudi R, Van Wanrooij MM, Van Opstal AJ. Audio-visual integration in a redundant target paradigm: a comparison between rhesus macaque and man. *Front Syst Neurosci*. 2017;11:89. https://doi.org/10.3389/fnsys.2017.00089
43. Broadway DC. Visual field testing for glaucoma – a practical guide. *Community Eye Health*. 2012;25:66–70.
44. Drance SM. The early field defects in glaucoma. *Invest Ophthalmol Vis Sci*. 1969;8:84–91.
45. Weinreb RN, Aung T, Medeiros FA. The pathophysiology and treatment of glaucoma: a review. *JAMA*. 2014;311:1901–11.
46. Hu CX, Zangallu C, Hsieh M, Gupta L, Williams AL, Richman J, et al. What do patients with glaucoma see? Visual symptoms reported by patients with glaucoma. *Am J Med Sci*. 2014;348:403–9.

47. Kadavath Meethal NS, Mazumdar D, Asokan R, Panday M, Van der Steen J, Vermeer KA, et al. Development of a test grid using eye movement perimetry for screening glaucomatous visual field defects. *Graefes Arch Clin Exp Ophthalmol*. 2018;256:371–9.

How to cite this article: Chanakya AVR, Bremen P. Optimising reaction-time analysis in eye movement perimetry using pooled promptness distributions. *Ophthalmic Physiol Opt*. 2025;00:1–21. https://doi.org/10.1111/opo.13564

APPENDIX A

SYNCHRONISATION OF TARGET PRESENTATION AND EYE-TRACKING TIMING

The synchronisation between the screens, that is, target presentation and eye tracker of the haploscopic system was characterised as follows. A Photron High-Speed Camera (Photron Fastcam Nova S16 type 1100K-M-64GB 10GbE model, photron.com) was positioned behind the participant so that it could concurrently image (1000 frames/s) the targets presented on the screen and the participant's eyes via two mirrors placed between the monitor and the participant. In addition, the Tobii X3-120 eye tracker was used to measure eye movements. This allowed direct comparison of the reaction times measured using the Photron and the Tobii systems. The infrared lights from the eye tracker caused overexposure of the camera sensor. To minimise lens flare, a Hoya UV and IR Cut 55 filter (Hoya Filter, Kenko Tokina Co., Ltd., hoya-filter.eu) was placed in front of the camera.

A measurement block consisted of a series of trials. A trial started with a white central fixation circle on a black background which the participant had to fixate. After an interval of 100 ms, a white target at either 15° horizontal, −8° vertical or 15° horizontal, +8° vertical appeared. The participant was instructed to make an eye movement towards the perceived target location. Each target was presented six times for a total of 12 trials per block. The total measurement time per block was about 50 s. We collected six blocks for left, right and both monitors together for a total of 36 repetitions per condition and target.

The data were downloaded from the camera as .jpeg format files via Photron FASTCAM Viewer software (version 4.2.0.0). All data analysis was conducted using MATLAB (version R2024a; MathWorks Inc., mathworks.com). To obtain the time course of the targets, pixels of interest were defined in the recorded images. For the eye image, the time traces were extracted by performing a principal components analysis in a user-defined area of interest around the eye. The second principal component described the eye position and could be used to extract reaction times as described in the 'Extraction of saccadic parameters' section. It was found that reaction times measured with the eye tracker were on average 18 ms slower (lower/upper 95% CI: 6/30 ms) than those obtained with the camera. The monitors did not affect the reaction time difference. Since the difference between the two systems varied unpredictably across the recording time, it was not possible to correct for this variable delay.